



Wavelength modulation spectroscopy near 5 μm for carbon monoxide sensing in a high-pressure kerosene-fueled liquid rocket combustor

Daniel D. Lee¹ · Fabio A. Bendana¹ · S. Alexander Schumaker² · R. Mitchell Spearrin¹

Received: 31 January 2018 / Accepted: 3 April 2018 / Published online: 16 April 2018
© Springer-Verlag GmbH Germany, part of Springer Nature 2018

Abstract

A laser absorption sensor was developed for carbon monoxide (CO) sensing in high-pressure, fuel-rich combustion gases associated with the internal conditions of hydrocarbon-fueled liquid bipropellant rockets. An absorption feature near 4.98 μm , comprised primarily of two rovibrational lines from the P-branch of the fundamental band, was selected to minimize temperature sensitivity and spectral interference with other combustion gas species at the extreme temperatures ($> 3000\text{ K}$) and pressures ($> 50\text{ atm}$) in the combustion chamber environment. A scanned wavelength modulation spectroscopy technique (1f-normalized 2f detection) is utilized to infer species concentration from CO absorption, and mitigate the influence of non-absorption transmission losses and noise associated with the harsh sooting combustor environment. To implement the sensing strategy, a continuous-wave distributed-feedback (DFB) quantum cascade laser (QCL) was coupled to a hollow-core optical fiber for remote mid-infrared light delivery to the test article, with high-bandwidth light detection by a direct-mounted photovoltaic detector. The method was demonstrated to measure time-resolved CO mole fraction over a range of oxidizer-to-fuel ratios and pressures (20–70 atm) in a single-element-injector RP-2-GOx rocket combustor.

1 Introduction

Hydrocarbon-fueled liquid rocket engines (LREs) are used in many modern launch systems. The high propellant mass fractions and high payload costs of such systems drive an acute need to maximize the mass-specific thrust of the engine. Combustion performance is a principal factor in determining mass-specific thrust, or specific impulse, and is usually quantified by a characteristic velocity ($c^* = p_0 A^* / m$) attained by measurements of the chamber pressure and total mass flow rate [1]. Such measurements provide a convenient way to globally quantify the aggregate of multiple processes that occur in the combustion chamber (e.g., vaporization, mixing, reaction), but these measures lack the granularity

to quantify combustion progress in the spatial domain (i.e., pressure is nearly constant throughout the chamber). In contrast, knowledge of combustion gas species along the axis of flow in a rocket combustion device provides a means to assess combustion progress relative to equilibrium or a fluid dynamic model. Unfortunately, the harsh conditions internal to hydrocarbon-fueled rocket combustion devices present a uniquely difficult challenge for species measurements. In this paper, we describe a novel approach for in situ detection of carbon monoxide in high-pressure liquid rocket combustors based on mid-infrared laser absorption spectroscopy.

Despite recent advancements in laser absorption spectroscopy (LAS) for studies of air-breathing propulsion systems, there have been very few attempts in developing and applying LAS measurement schemes to rocket propulsion devices. Previous efforts include exhaust plume tomography of water vapor by Caswell et al on a $\text{CH}_4\text{-GO}_x$ rocket motor using a near-infrared (IR) external cavity diode laser [2], near-IR measurements of ammonia and water vapor by Makowiecki et al in a simulated hydrazine thruster plume [3], near-IR water vapor detection by Locke et al in a $\text{GH}_2\text{-GO}_x$ rocket combustor up to 8 atm [4], and infrared measurements of multiple species (N_2O , NO , and CO) by Zeng et al in an ammonium dinitramide-based thrust chamber near 7 atm [5]. Only the latter two works involved

This article is part of the topical collection “Mid-infrared and THz Laser Sources and Applications” guest edited by Wei Ren, Paolo De Natale and Gerard Wysocki.

✉ Daniel D. Lee
daniellee9101@ucla.edu

¹ Department of Mechanical and Aerospace Engineering, University of California Los Angeles, Los Angeles, CA 90095, USA

² U.S. Air Force Research Laboratory, Edwards Air Force Base, Kern County, CA 93524, USA

LAS measurements of species internal to a rocket combustion chamber and at pressures above ambient. Significantly more effort has been committed to LAS applications in air-breathing propulsion, including higher pressure environments (> 10 atm). Notable previous works include H_2O measurements in the near-infrared in a gas turbine combustor at pressures up to 30 atm by Caswell et al [6] and mid-infrared detection of H_2O and CO above 40 atm in a pulse detonation engine by Goldenstein et al [7] and Spearin et al [8]. This latter mid-infrared work has informed the design and advancement of the current CO sensor for rocket applications.

Notable differences exist between air-breathing systems and rocket propulsion systems that use similar hydrocarbon fuels, and these differences impact sensor design and operability. Table 1 provides a comparison of representative conditions in a typical kerosene-fueled rocket and gas turbine combustor, respectively. While both systems are designed to minimize the onboard mass of propellants per unit thrust, rockets carry both fuel and oxidizer whereas air-breathing systems carry only the fuel. Air-breathing combustors thus typically burn fuel-lean, whereas rockets usually burn fuel-rich to maximize specific impulse. This results in extensive soot formation in the fuel-rich combustion of conventional hydrocarbon rocket fuels (i.e., kerosene) [9]. Without the added heat capacity of nitrogen, rockets also reach much higher combustion temperatures ($T > 3000$ K), and the acute need for high thrust demands higher chamber pressures ($P > 50$ atm). The extreme thermodynamic conditions typical of hydrocarbon-fueled rocket combustion generally increase spectral interference through band and line broadening [10]. Sooting associated with fuel-rich combustion leads to beam scattering and window fouling. Differences in oxidizer-to-fuel ratio, combined with the lack of nitrogen, also yields a unique rocket gas composition and associated spectra from which to probe. With these factors in

Table 1 Example conditions of RP-1-LOx (rocket) and JP-4-Air (gas turbine) combustion gases with representative broadening coefficients of gas components perturbed by nitrogen

	RP-1- LOx	JP-4- Air	$2\gamma_{i-N_2}(300K)$ [cm ⁻¹ /atm]
ϕ	1.35	0.8	
T_{\max}	3600 K	2000 K	
P_{\max}	> 50 atm	25 atm	
N_2	–	74%	–
CO	35%	$< 1\%$	0.13
CO ₂	12%	11%	0.15
H ₂ O	32%	10%	0.23
OH	4%	$< 1\%$	0.15
O ₂	$< 1\%$	4%	–
H ₂	11%	$\ll 1\%$	–

mind, a unique sensing strategy is required for species measurements in hydrocarbon-fueled rockets. In the following sections, we detail the CO sensor design and development, from theoretical approach to demonstration on a kerosene-fueled rocket combustor.

2 Theory

2.1 Absorption spectroscopy

The theory of absorption spectroscopy has been thoroughly discussed in previous works [11, 12] and will only be briefly outlined to describe the analytical approach and introduce notation. The fundamental relationship governing LAS measurements is the Beer-Lambert law given by Eq. 1, which relates thermodynamic gas properties and mole fraction, x_{abs} , to incident light intensity (I_0) and transmitted light intensity (I_t) over the optical path length, L .

$$\alpha_\nu = -\ln\left(\frac{I_t}{I_0}\right)_\nu = \sum_i x_{abs} S_i(T) \varphi(\nu, T, P, x_{abs}) L \quad (1)$$

In projecting monochromatic light across a gas medium (i.e., rocket combustor), the ratio of light intensities can be measured to determine the spectral absorbance, α_ν , of molecules with quantum energy transitions resonant at the optical frequency, ν . The spectral absorbance can then be directly related to the thermodynamic gas properties and mole fraction of the absorbing molecule through the spectral line-strength, $S_i(T)$, and line-shape function, $\varphi(\nu, T, P, x_{abs})$. Developing an LAS sensor for species measurements in high-pressure and high-temperature environments requires an accurate accounting of these spectroscopic parameters for each line i that contributes to the local spectra.

The spectral line-shape can generally be well represented by accounting for Doppler and collisional broadening, which capture temperature and pressure dependencies, respectively, with an appropriate line-shape function (e.g., Voigt). Collisional broadening has a pronounced effect at the high pressures associated with rocket combustion, leading to undesirable blending of neighboring lines, or spectral interference, as well as reduced differential absorption that limits range. This broadening effect is represented by a collisional line-width, $\Delta\nu_c$, defined in Eq. 2. Here, $2\gamma_{abs-j}$ is the collisional broadening coefficient between perturbing species j and the absorbing species, and is specific to each line i . Its temperature dependence is typically captured by a power law (Eq. 3).

$$\nu_c = P \sum_j x_j 2\gamma_{abs-j} \quad (2)$$

$$\gamma_i(T) = \gamma_i(T_0) \left(\frac{T_0}{T}\right)^n \quad (3)$$

To minimize the detrimental effects of line broadening, and maximize pressure range, a molecule with a low collisional broadening coefficient is advantageous. The molecular dependence of collisional broadening can be distilled to the optical collision diameter and reduced mass, $\gamma \sim d_{ij}^2 \sqrt{\mu_{ij}}$, such that a combination of small size and large mass is desired [10].

Table 1 compares representative collisional broadening coefficients for the various components of hydrocarbon combustion gases. First we note that the homonuclear diatomics are not infrared active. Fortunately, in contrast to lean air-breathing systems, the high-temperature fuel-rich conditions of hydrocarbon fueled rockets provide for a large fraction of infrared active diatomic species in the equilibrium combustion product mixture. The most abundant of these species is CO, which also exhibits a comparatively low collisional broadening coefficient relative to the other infrared active species (CO_2 , H_2O , OH), resulting from a smaller optical diameter than the larger polyatomic species, and a larger molecular mass than OH. Consequently, CO can have substantially less collisional broadening at high pressures typical of modern rocket propulsion systems, which lessens the interference of neighboring lines, preserves differential absorption, and provides a theoretical basis for LAS measurements in rocket combustion flows above the pressure limits of previous works discussed in Sect. 1.

2.2 Scanned wavelength modulation spectroscopy

A scanned-wavelength modulation spectroscopy (WMS) technique, with normalized second harmonic ($2f$) detection, was employed in this work to measure the absorption of carbon monoxide. Scanned-WMS has proven advantageous in harsh environments where entrained particles lead to substantial raw signal noise (scattering and beam steering) and at high pressures (> 50 atm) where the signal absolute baseline is unavailable [11, 13]. Measurements are conducted by rapidly injection-current tuning the laser with a high-frequency sinusoidal waveform superimposed on a lower frequency waveform to modulate wavelength over the target absorption feature. The raw detector signal is post-processed through a lock-in amplifier and frequency filtered to isolate the second harmonic ($2f$) of the modulation frequency, which is sensitive to spectral line-shape curvature and can be compared to a spectral model to infer gas properties. The slower scan is used to attain spectral resolution of the harmonic signals. The method is convenient for eliminating noise at frequencies outside a prescribed passband, set by the selection of the modulation frequency and frequency filter. Additionally, $1f$ -normalization of the $2f$ signal eliminates the dependency on laser intensity variation due to emission

and non-absorbing transmission losses [14], important for a high-temperature sooting environment.

In scanned-WMS, the optical output frequency of the laser, $\nu(t)$, can be modeled with Eq. 4, where $\bar{\nu}_L$ represents the center frequency/wavenumber of the modulation, a_S and a_M are the amplitudes or depths of the slow scan and modulation waveform, f_S and f_M are the scan and modulation frequencies, and ψ_S and ψ_M are the corresponding phase shifts.

$$\nu(t) = \bar{\nu}_L + \nu_S(t) + \nu_M(t) = a_S \sin(f_S t + \psi_S) + a_M \sin(f_M t + \psi_M) \quad (4)$$

The user has some control in prescribing these parameters, subject to laser tuning characteristics, which directly affect the harmonic signal strength and signal-to-noise ratio (SNR) of the species measurement. Section 4 discusses the approach used to determine modulation settings for the rocket combustor application and the spectral model from which species concentration is inferred by comparison to the WMS measurement. First, Sect. 3 describes the wavelength selection that prescribes $\bar{\nu}_L$.

3 Wavelength selection

For the target measurement, there are three primary criteria for wavelength selection: (1) strong differential absorption within the laser tuning range, which translates to a large WMS- $2f$ signal, (2) minimal interference with other combustion species, namely carbon dioxide and water, and (3) temperature insensitivity. The strongest CO absorption in the infrared occurs near the fundamental vibrational frequency (2140 cm^{-1}), and this mid-infrared domain has recently become accessible with room-temperature quantum cascade lasers that can implement rapid tuning techniques (e.g. scanned-WMS). Figure 1 shows the fundamental CO absorption band centered near $4.7 \mu\text{m}$ with the neighboring CO_2 and H_2O absorption bands within the surrounding domain of $4.1\text{--}5.7 \mu\text{m}$. This relatively broad spectral line-strength

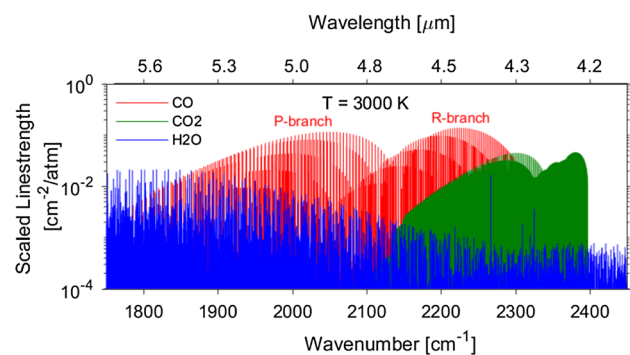


Fig. 1 Absorption line-strengths of CO, CO_2 , and H_2O at 3000 K (HITEMP [15])

survey at 3000 K indicates regions of the CO band that may be favorable for low interference measurements in a high-temperature rocket environment. The dense CO₂ spectra, comprised of many lines and small line spacing, interferes substantially with the R-branch of CO at frequencies above 2100 cm⁻¹. The H₂O spectrum similarly overlaps with CO throughout the domain of interest, but is less crowded compared to the CO₂ band. The larger spacing between water lines allows for some potentially low-interference spectral windows, and indicates the lower-frequency P-branch of CO as a favorable domain.

Within the P-branch of the fundamental CO band, the spectral lines near 2060 cm⁻¹ have been utilized previously for LAS sensing in air-breathing propulsion flows [7, 16], and this wavelength was initially considered for the current work. However, detailed absorption simulations suggest that the much higher temperatures and pressures expected in the rocket environment introduce substantial CO₂ interference at this wavelength associated with a combination of Boltzmann broadening of the neighboring CO₂ $\bar{\nu}_3$ band with increased temperature and individual line broadening with increased pressure. To avoid this CO₂ interference, we look to lower frequencies in the P-branch. Figure 2 shows an absorption simulation, using the HITEMP spectroscopic database [15], of a representative condition for kerosene-oxygen rocket combustion at 60 atm at select spectral domains near 4.9 μm . This figure highlights the CO₂ interference near 2060 cm⁻¹. Note that thermochemical properties, as assigned in the absorption simulation, have been estimated using the NASA Chemical Equilibrium with Applications (CEA) tool.

A survey of the remainder of the simulated spectrum in the domain of 1950–2100 cm⁻¹ revealed the CO absorption feature near 2008 cm⁻¹ as an attractive target (also shown in Fig. 2) [17]. The local absorption is primarily comprised of two rovibrational transitions which blend into one spectral feature at elevated pressure. The P(31) line in the $\nu(0\rightarrow 1)$ fundamental band makes the dominant contribution but the

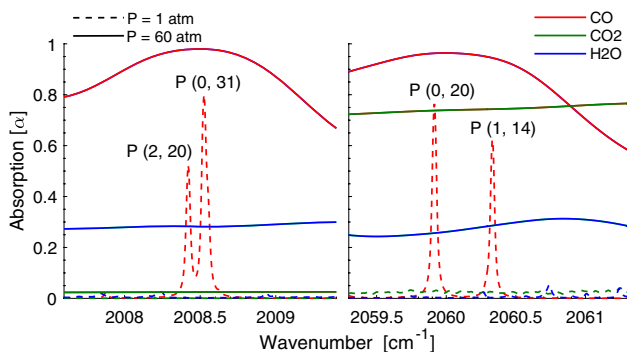


Fig. 2 Absorption simulations near 2008 and 2060 cm⁻¹ at expected equilibrium condition; $T = 3500$ K, $X_{\text{CO}} = 0.3$, $X_{\text{CO}_2} = 0.15$, $X_{\text{H}_2\text{O}} = 0.35$, $L = 2.54$ cm

P(20) line in the $\nu(2\rightarrow 3)$ hot band also contributes at most expected conditions. To a lesser degree, the neighboring P(26) line near 2006.8 cm⁻¹ in the $\nu(1\rightarrow 2)$ band makes a contribution above 50 atm. Most notably, the domain near 2008 cm⁻¹ has significantly less CO₂ interference than 2060 cm⁻¹, and H₂O interference is similar with negligible differential H₂O absorption. In addition to less interference, differential CO absorption is also slightly stronger at 2008 cm⁻¹ at the target high-pressure condition, as broadening coefficients for these higher rotational quanta (J) lines are smaller. Due to these advantages, the CO absorption feature near 2008 cm⁻¹ was selected for this sensing application. Table 2 specifies the relevant spectroscopic line parameters in this domain, taken from the HITEMP database and from the experimental and modeling work of Hartmann et al [18]. In modeling the spectra, a Voigt line-shape function is used, which has been shown to be suitable at similar gas densities for other CO lines within the fundamental band [8]. In calculating line broadening, the gas composition is approximated from thermochemical calculations. As table 2 indicates, broadening coefficients are available for most collision partners. For the 10–15% of species for which broadening data is not available (e.g., OH, H₂, radicals), the broadening per unit pressure is assumed to equal that of the balance gas.

As for the final wavelength selection criteria, low temperature sensitivity is desired to minimize influence of temperature uncertainty. It is found that the high lower state

Table 2 Spectroscopic line assignments and collisional-broadening for the CO lines of interest [18] [19]

P (ν' , J'')	P (0,31)	P(2,20)	P(1,26)
ν_0 (cm ⁻¹)	2008.53	2008.42	2006.78
E'' (cm ⁻¹)	1901.1	5051.7	3477.6
S (cm ⁻² /atm)	6.48×10^{-3}	2.78×10^{-9}	5.09×10^{-6}
CO–H ₂ O			
γ	94.9	119	106
n	0.61	0.71	0.66
CO–CO ₂			
γ	40.2	51.8	44
n	0.47	0.5	0.48
CO–N ₂			
γ	40.9	52.2	46.3
n	0.47	0.57	0.52
CO–CO			
γ	43	55	48
n	0.5	0.5	0.5
CO–O ₂			
γ	43.2	46.9	45
n	0.56	0.56	0.56

Note: γ (300 K) in units of $10^{-3} \times (\text{cm}^{-1}/\text{atm})$ and S at 296 K

energies of the lines near 2008 cm^{-1} lend to low temperature sensitivity. This is discussed in the context of measurable WMS signals in Sect. 4.

4 Sensor development

This section describes key elements of sensor development required for successful application of the spectroscopic sensor design. These elements include the refinement of laser control and tuning parameters, spectral modeling and interpretation of the WMS harmonic signals, optical engineering, and facility interface and setup.

4.1 Optimizing laser tuning parameters

Within the framework of scanned-WMS, the tuning depths (a_S and a_M) and frequencies (f_S and f_M) can be adjusted to optimize signal quality (i.e., signal-to-noise ratio) for a given gas condition or application environment. A basic analytical model based on laser tuning characteristics, measured in the laboratory, can be used to simulate WMS harmonic signals and inform parameter optimization [13]. Two guiding principles in the selection of these parameters should be noted: (1) Maximizing the WMS- $2f$ generally maximizes signal-to-noise ratio, and this signal increases with the level of differential absorption spanned during wavelength modulation. At high-pressures where laser tuning range is often limited to a fraction of the absorption line-width, the WMS- $2f$ tends to increase monotonically with modulation depth [19]. (2) Modulating at higher frequencies enables higher time resolution measurements and tends to improve noise rejection. Time resolution or sensor bandwidth is determined by the passband frequency which is a prescribed fraction of the modulation frequency. Additionally, mechanical noise in the system (vibrations, beam steering, etc.) tends to be more intense at relatively low frequencies ($< 10\text{ kHz}$) and can be avoided by shifting the absorption information to higher frequencies, thus improving SNR. Unfortunately, laser tuning depth has an inverse relationship with frequency, and thus a compromise is required between the competing demands of signal quality and time-resolution.

Figure 3 shows the maximum modulation depth versus frequency for the quantum cascade laser used in this work. The maximum modulation depth is determined at each frequency by inputting the maximum injection current range permitted, and measuring the relative wavenumber achieved calibrated against the free-spectral range of a germanium etalon, through which the light is projected. Maximum modulation depth is shown to decrease logarithmically with frequency. Additionally, the benefit of using a large modulation depth for this high-pressure application is illustrated in figure 4 by simulations of the relative WMS- $2f$ signal (at

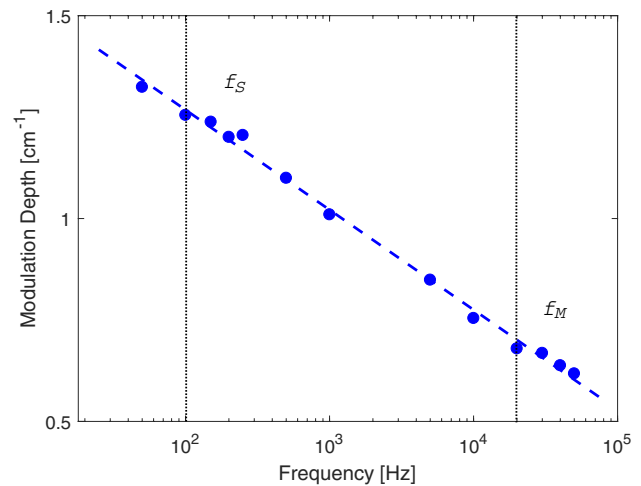


Fig. 3 Measured modulation depth at maximum injection current amplitude ($\pm 45\text{ mA}$) as a function of laser modulation frequency

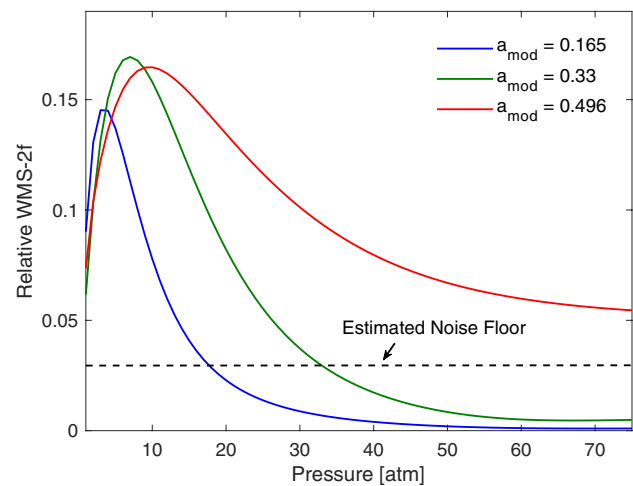


Fig. 4 Simulated WMS- $2f$ (background subtracted) near 2008 cm^{-1} as a function of pressure for various modulation depths at expected equilibrium; $T = 3500\text{ K}$, $X_{\text{CO}} = 0.32$, $L = 2.54\text{ cm}$

2008.52 cm^{-1}) versus pressure at different modulation depths achievable with the laser. Modulating at a depth greater than 0.4 cm^{-1} is shown to enable significantly expanded pressure range for the sensor. It should be noted that mid-infrared quantum cascade lasers have improved considerably in current tuning range in recent years, underlying this advancement in capability. Nevertheless, a trade-off between tuning frequency and signal strength is evident

Adding a low frequency waveform to the high frequency modulation in order to spectrally resolve the harmonic signals reduces the available injection current for modulation, and therefore should be minimized in scan depth. The main purpose of the slow scan in this application is to ensure that a local peak is measured, allowing for some uncertainty in

pressure shifting of the target transitions. In this case, fully resolving the harmonic spectra is not required, and a low-amplitude dithering of the slow scan (i.e., small a_s) over the local peak is acceptable. For the present work, a scan depth and frequency of 0.141 cm^{-1} and 100 Hz were selected, respectively, to capture the local $2f$ peak signal associated with the absorption feature. With the remaining injection current budget, a modulation depth and frequency of 0.496 cm^{-1} and 20 kHz were chosen to yield adequate WMS- $2f$ signal strength at the highest possible frequency.

4.2 Simulation of scanned WMS harmonic signals

To infer species concentration, a model is required to compare simulated signals (in which species concentration is an input), to measured signals. Here, we follow the approach of Sun et al. [20], in which a measured background laser intensity (I_0), at the scanned-WMS settings, is combined with a simulated absorbance versus time function, using $\nu(t)$ per Eq. 4, to generate a simulated laser transmission signal ($^S I_t$). The simulated absorbance spectrum is created using the spectroscopic parameters detailed in Sect. 3, and the optical frequency response $\nu(t)$ is characterized in the laboratory, and contains the selected laser tuning parameters ($f_s = 100 \text{ Hz}$ and $a_s = 0.141 \text{ cm}^{-1}$, $f_M = 20 \text{ kHz}$ and $a_M = 0.496 \text{ cm}^{-1}$). The simulated transmitted intensity ($^S I_t$), can then be processed through a digital lock-in amplifier and low-pass filter in the same manner as the measured transmitted intensity ($^M I_t$). The lock-in analysis extracts the WMS harmonic signals which can be compared between the simulation and measurement, after background subtraction and normalization.

The simulation process at the scanned-WMS settings used in this work is illustrated in Fig. 5. The measured background laser intensity (I_0) is shown in blue with a 20 kHz modulation frequency. Simulated transmission signals at a representative condition (30 atm) for the kerosene-oxygen rocket combustor are also shown at two different input values of CO mole fraction (red and green) and reflect the molecular absorption. The corresponding background-subtracted WMS- $2f/1f$ harmonic signals, extracted from lock-in analysis of these transmission signals, are shown in the lower sub-figure. This sub-figure also shows the variation of the harmonic signals at 100 Hz where the slower scan crosses over the local WMS- $2f/1f$ peaks. This simulation method is used to infer species abundance by iterating mole fraction to converge the simulated signal with measurement, as will be shown in Sect. 5.

With a complete spectral model, we now revisit the temperature sensitivity of the measurement technique. At the selected laser settings, we iterate the simulation process over a range of possible temperatures and pressures in the rocket combustor, generating a matrix of WMS harmonic

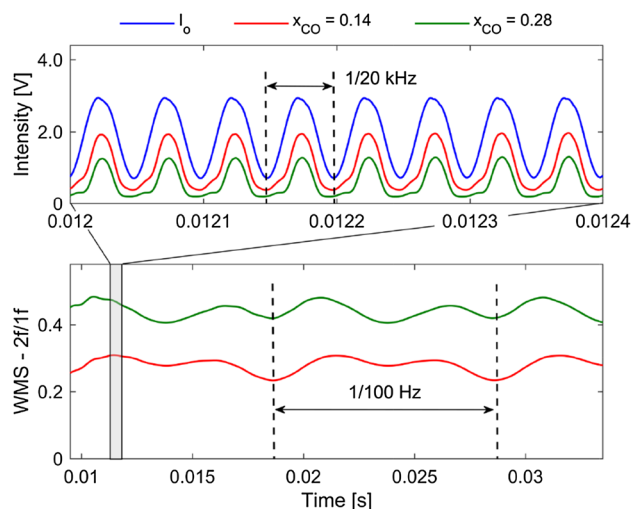


Fig. 5 Scanned-WMS intensity signals with simulated absorbance at different X_{CO} (top), and corresponding WMS- $2f/1f$ harmonic signals after lock-in extraction (bottom); $P = 440 \text{ psi}$ (30 atm), $T = 3570 \text{ K}$, $L = 2.54 \text{ cm}$

signals, from which a numerical derivative of the WMS- $2f$ can be taken with respect to temperature at any given condition. Normalizing this derivative with respect to the signal magnitude and temperature [i.e., $(dS/S)/(dT/T)$], we can determine the uncertainty of the measured WMS- $2f$ resulting from an uncertainty in temperature on a percentage basis. It can be shown that CO mole fraction is approximately linearly proportional to the WMS- $2f$ signal such that the derivative can approximate the sensitivity of the inferred CO concentration measurement to temperature.

This numerical calculation, conducted as a function of temperature from $800\text{--}3700 \text{ K}$ at distinct pressures, is shown in the lower sub-plot of Fig. 6. The respective line-strengths of the three most dominant transitions that comprise the absorption feature are also shown as a function of temperature (in the upper sub-plot) to assist in interpretation of the temperature sensitivity. For all pressure conditions, temperature sensitivity decreases significantly until it reaches zero where the local WMS- $2f$ reaches a maximum. This generally correlates to the maximum of differential absorption related to the summation of contributing line-strengths. The zero point shifts to higher temperatures as pressure increases mainly due to a change in relative contribution from the three transitions. At 25 atm , the P(0, 31) makes the dominant contribution to the signal strength, while at 50 and 70 atm , the P(1, 26) and P(2, 20) lines contribute more substantially. At temperatures above the inflection point, the temperature sensitivities remain low as line-strengths decrease gradually. At the primary conditions of interest ($2000\text{--}3700 \text{ K}$) the temperature sensitivity is mostly less than 0.5 at all pressures. This may

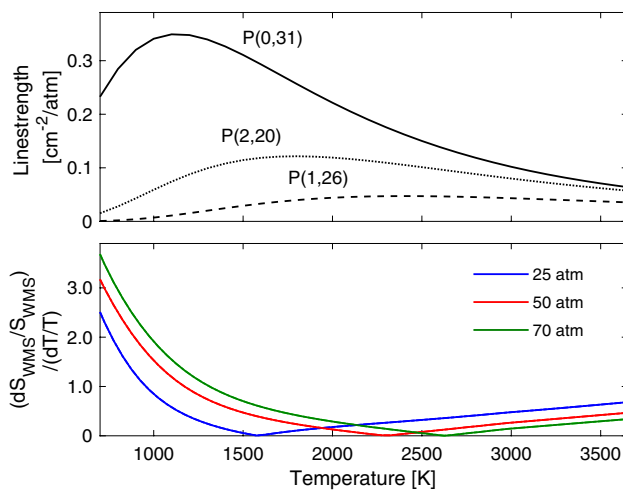


Fig. 6 Line-strength and temperature sensitivity of WMS- $2f$ signal (background subtracted) near 2008 cm^{-1} as a function of temperature for various pressures; $a_{\text{mod}} = 0.496\text{ cm}^{-1}$

be interpreted as estimating that a $\sim 10\%$ uncertainty in temperature would yield a $\sim 5\%$ uncertainty in species.

5 Experimental setup

In this section we detail the sensor hardware and interface with the liquid rocket test article. Figure 7 provides a schematic representation of the integration. The total length of the combustion chamber is approximately 35 cm with a square cross-section of 6.45 cm^2 area. Measurements are taken across a 2.5 cm transverse optical path-length located 32 cm downstream of the single-element injector.

A distributed-feedback quantum cascade laser with $\sim 50\text{ mW}$ output power is used as the single-mode light source to probe the target CO absorption feature near 2008.5 cm^{-1} . The beam is free-space coupled into a hollow-core fiber (2 m length) for remote light delivery using a calcium fluoride coupling lens with a focal length of 100 mm and a multi-axis

stage for optical alignment [21]. The fiber output is then re-collimated using another calcium fluoride lens and pitched across the combustion chamber (4 mm aperture) through two wedged sapphire windows (3/8 in. diameter with 1° wedge), which were recessed $\sim 50\text{ cm}$ from the combustion flow path. The beam diameter was estimated to be $\sim 2\text{ mm}$ upon re-collimation. The transmitted light is spectrally filtered to reduce thermal emission and is collected on a thermo-electrically cooled photovoltaic (PV) detector. Both the pitch and catch optics were mounted on kinematic mounts to optimize alignment and maximize the transmitted light intensity during the experiment.

The DFB laser was injection-current tuned to be centered near 2008.52 cm^{-1} and was driven by a scanning sinusoid at 100 Hz and modulation sinusoid at 20 kHz . The respective modulation depths used were 0.141 and 0.496 cm^{-1} , allowing a maximum wavelength scan range of 0.637 cm^{-1} to partially resolve the pressure-broadened transitions illustrated in Fig. 2. Raw detector voltage data were typically collected at a sample rate of 5 MS/s in 5-s intervals. Test article hot-fire tests usually spanned 2–3 s in duration.

To mitigate issues associated with the harsh thermo-mechanical environment, a number of practical methods were required to ensure successful sensor deployment on the rocket combustor. To displace excessive water vapor in the optical path that could spectrally interfere with CO measurements, nitrogen was fed into the fiber-optic and pitch assembly to purge the hollow-core fiber. Another practical issue was soot deposition on the sapphire windows. A helium purge system was employed in front of the wedged sapphire windows to keep the windows and recess volume clear. The helium purge pressure was iteratively adjusted to be just high enough such that soot formation was not observed (per window inspection between tests), minimizing the penetration depth of the helium into the combustion chamber [9]. Additionally, to counter mechanical vibrations and acoustic perturbations, the laser was mounted to a honeycomb vibration-dampening breadboard and the hollow-core fiber was mechanically supported by a structural shroud. Lastly, due

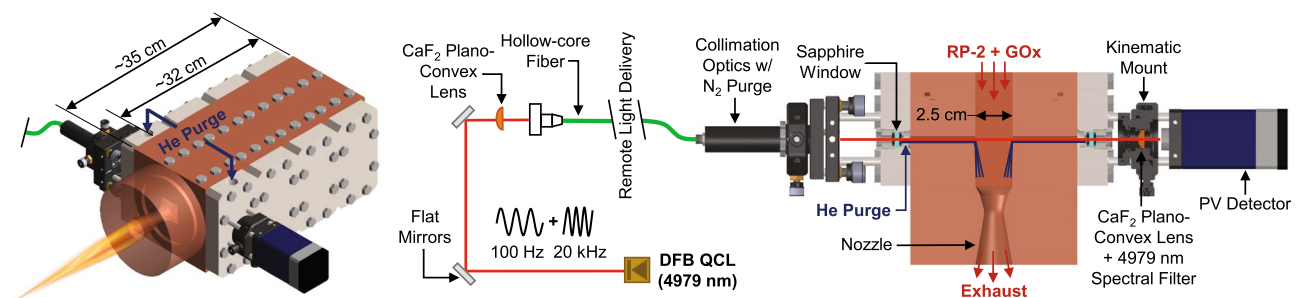


Fig. 7 Optical interface with RP-2-GOx rocket combustor for high-pressure CO sensing measurements. Graphical depiction of remote-light delivery and collection optics along with implemented He/N₂ purge systems

to thermal radiation from the combustor and ambient environment, the photovoltaic detector was mounted to a water-cooler plate to prevent saturation or overheating damage.

6 Sensor demonstration

Initial sensor application occurred at a bipropellant rocket test facility at the Air Force Research Laboratory in Edwards, CA. The facility is used, amongst other purposes, for assessment of the combustion characteristics of hydrocarbon rocket propellants and various injector designs. For the demonstration testing discussed here, kerosene (RP-2) and oxygen were used as the propellants. In situ CO species measurements were conducted in the combustion chamber over a pressure range of 25–70 atm and at oxidizer-to-fuel ratios ranging from 2.5–4.5. The combustion chamber is a stackable modular design, and the optical section was located at the furthest downstream location where chemical equilibrium is most likely achieved, providing a reference point for the measurements. Here we discuss a subset of the data collected to highlight species measurement capability.

Figure 8 shows an example test where chamber pressure and O/F ratio reached 58 atm and 2.59, respectively. The sub-figures show the time-resolved measurements of the WMS- $2f/1f$ signal and pressure along with the inferred species measurement. To infer CO mole fraction, temperature was estimated by thermochemical calculation while chamber

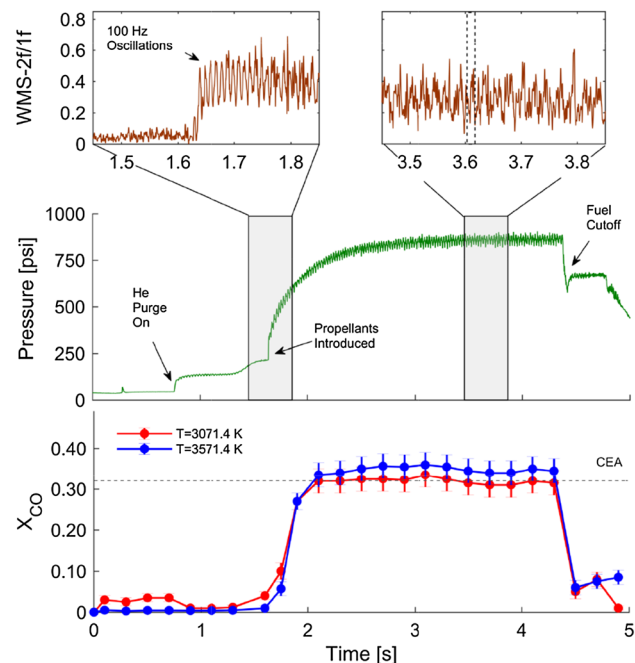


Fig. 8 Time evolution of chamber pressure, WMS- $2f/1f$ signal (background subtracted), and measured X_{CO} in RP-2-GOx combustor; O/F = 2.59

pressure was accurately measured via a pressure transducer. From the figure, we can observe the abrupt increase in WMS signal around 1.6 s, corresponding to the introduction of propellants and ignition. The WMS signal then decreases as pressure increases. Prior to ignition there is an increase in chamber pressure associated with the helium purge gas which is decreased thereafter. Maximum CO concentration occurs at around 3.1 s and decreases slightly as the combustor reaches steady state. The concentration measurement at steady state shows good agreement (10%) with equilibrium, calculated to yield $X_{\text{CO}} = 0.32$ at the measured chamber pressure and equivalence ratio (NASA CEA). Precision error is estimated to be $\sim 9\%$ in this case, an inverse of the signal-to-noise ratio. In order to estimate uncertainty introduced by the lack of a temperature measurement, CO concentration was calculated under two assumed temperature profiles ($T_{\text{eq}} = 3570$ K and 3070 K). Concentration uncertainty from this estimated temperature uncertainty is 10% from ignition to the end of combustion given the low temperature sensitivity of the measurement.

In Fig. 9, an averaged WMS- $2f/1f$ measurement in the steady state region at two distinct pressures is compared to simulated signals using the WMS model discussed in Sect. 4, assuming equilibrium temperature and floating mole fraction. A passband filter of 2 kHz was implemented with lock-in analysis of the harmonics (gray), whereafter 19 scans of the measurements during the steady state condition were also averaged (blue) to improve SNR. There are a few notable differences between the two measurements. SNR was ~ 7 and ~ 22 for the measurements at 1016 psi and 550

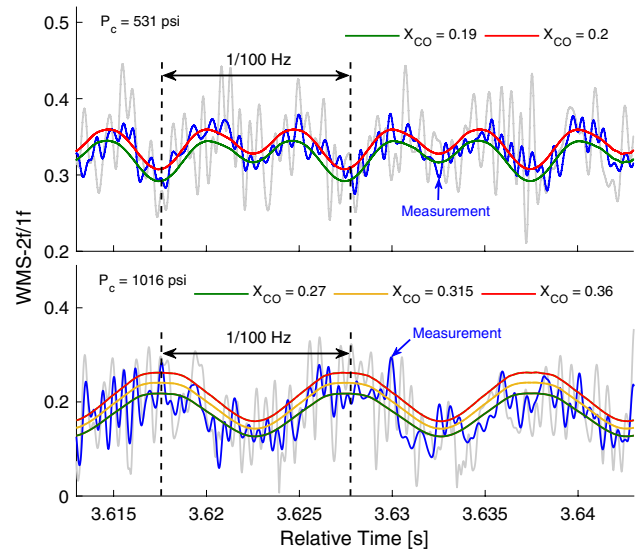


Fig. 9 Measured WMS signal shown with simulated WMS signals at $P = 531$ psi, $T = 3602$ K and $L = 2.54$ cm (top) and measured WMS signal shown with simulated WMS signals at $P = 1016$ psi, $T = 3674$ K, and $L = 2.54$ cm (bottom)

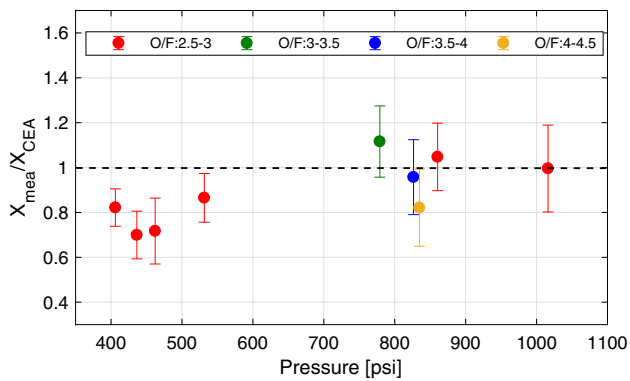


Fig. 10 Measured CO mole fraction compared to equilibrium CO mole fraction over range of pressures and O/F ratios

psi, as signal magnitude generally decreases with pressure as expected. Accordingly, the precision error is estimated to be ~ 15 and $\sim 5\%$, respectively. Another apparent difference is shape. The WMS- $2f/1f$ signal at 550 psi shows a local maximum in both the up scan and down scan. By contrast, the WMS signal at 1016 psi does not reveal this feature primarily due to the extreme pressure broadening of the absorbance spectrum that diminishes this local peak. In either case, the model and measurement are consistent with the evolution of the signal shape and gives confidence in the broadening model.

The post-processing method described above was applied to data from different test conditions to assess the level of agreement between the measurements in the steady state region and equilibrium conditions calculated via thermochemical analysis [NASA CEA]. Error bars are applied that combine the measurement noise with uncertainty related to temperature and spectroscopic model inputs via a simple sum of square errors. Typical uncertainties were ~ 10 – 15% . Figure 10 shows that the X_{CO} measurement agrees well with chemical equilibrium at most conditions, especially over 700 psi. There is greater disagreement, beyond the estimated measurement uncertainty, at lower pressures (550 psi) and this is suspected to be a consequence of the helium purge penetrating further into the chamber than intended and effectively decreasing the optical path-length along the line of sight. Future work in optimizing the purge system geometry may help minimize this effect.

7 Summary

A mid-infrared laser absorption sensor was developed for in situ measurements of nascent carbon monoxide at practical chamber conditions of hydrocarbon-fueled rockets. The sensor is enabled by novel wavelength selection in the CO fundamental band near $4.98 \mu\text{m}$ with strong differential

absorption, low temperature sensitivity, and minimal interference. A scanned wavelength modulation spectroscopy technique, leveraging recent enhancements in tuning response of quantum cascade lasers, provided for quantitative signal recovery and interpretation despite large non-absorption raw signal losses, unavailable baseline signal caused by high collisional broadening, and noise associated with vibrations and emission during facility operation. Time-resolved field measurements of CO mole fraction were successfully conducted at relevant pressures and oxidizer-to-fuel ratios on a kerosene-oxygen rocket combustor at the Air Force Research Laboratory in Edwards, CA. To the authors' knowledge, these data represent the first quantitative species measurements in a hydrocarbon-fueled rocket combustion chamber at realistic operating conditions (> 40 atm), and an extension in pressure range (up to 70 atm) for laser absorption combustion diagnostics more generally. The advantageous features of the CO sensing strategy provide for broad utility in high-pressure, fuel-rich combustion studies.

Acknowledgements This work was sponsored by the Air Force Research Laboratory in Edwards, CA under Award No. 16-EPA-RQ-09. The authors thank Dr. Ed Coy and Dr. Steve Danczyk of AFRL for their support in conducting field measurements.

References

- P.G. Hill, C.R. Peterson, *Mechanics and thermodynamics of propulsion*. 2nd edn. (Addison-Wesley Publishing Co, Reading, 1992)
- A.W. Caswell, S.T. Sanders, M.J. Chiaverini, 41st AIAA/ASME/SAE/ASEE Joint Propulsion Conference & Exhibit (2005)
- A.S. Makowiecki, T.R. Hayden, M.R. Nakles, N.H. Pilgram, N.A. MacDonald, W.A. Hargus, G.B. Rieker, 53rd AIAA/SAE/ASEE Joint Propulsion Conference (2017)
- J. Locke, S. Pal, R. Woodward, R. Santoro, 49th AIAA Aerospace Sciences Meeting including the New Horizons Forum and Aerospace Exposition (2011)
- H. Zeng, F. Li, X. Yu, D. Ou, L. Chen, *Appl. Opt.* **57**, 1321 (2018)
- A.W. Caswell, K. Rein, S.T. Sanders, T. Kraetschmer, S. Roy, D.T. Shouse, James R. Gord, *Appl. Opt.* **49**, 4963 (2010)
- C.S. Goldenstein, R.M. Spearrin, J.B. Jeffries, R.K. Hanson, *Proc. Combust. Inst.* **35**, 3739–3747 (2015)
- R.M. Spearrin, C.S. Goldenstein, J.B. Jeffries, R.K. Hanson, *Appl. Opt.* **117**, 689–698 (2014)
- E.B. Coy, 53rd AIAA Aerospace Sciences Meeting (2015)
- R.K. Hanson, R.M. Spearrin, C.S. Goldenstein, *Spectroscopy and Optical Diagnostics for Gases* (Springer, New York, 2016)
- C.S. Goldenstein, R.M. Spearrin, J.B. Jeffries, R.K. Hanson, *Progr. Energy Combust. Sci.* **60**, 132–176 (2017)
- M.G. Allen, *Measurement Sci. Technol.* **9**, 545–562 (1998)
- K. Sun, R. Sur, X. Chao, J.B. Jeffries, R.K. Hanson, R.J. Pummill, K.J. Whitty, *Proc. Combust. Inst.* **34**, 3593–3601 (2013)
- G.B. Rieker, J.B. Jeffries, R.K. Hanson, *Appl. Opt.* **48**, 5546 (2009)
- L.S. Rothman, I.E. Gordon, R.J. Barber, H. Dothe, R.R. Gamache, A. Goldman, V.I. Perevalov, S.A. Tashkun, J. Tennyson, *J. Quant. Spectrosc. Radiat. Transfer* **111**, 2139–2150 (2010)
- R.M. Spearrin, W. Ren, J.B. Jeffries, R.K. Hanson, *Appl. Phys. B: Lasers Opt.* **116**, 855–865 (2014)

17. C.S. Goldenstein, V.A. Miller, R.M. Spearrin, C.L. Strand, J. Quant. Spectrosc. Radiat. Transfer **200**, 249–257 (2017)
18. J.M. Hartmann, L. Rosenmann, M.Y. Perrin, J. Taine, Appl. Opt. **27**, 3063 (1988)
19. H. Li, G.B. Rieker, X. Liu, J.B. Jeffries, R.K. Hanson, Appl. Opt. **45**, 1052 (2006)
20. K. Sun, X. Chao, R. Sur, C.S. Goldenstein, J.B. Jeffries, R.K. Hanson, Measurement Sci. Technol. **24** (2013)
21. J.M. Kriesel, N. Gat, B.E. Bernacki, R.L. Erikson, B.D. Cannon, T.L. Myers, C.M. Bledt, J.A. Harrington, In *Chemical, Biological, Radiological, Nuclear, and Explosives (CBRNE) Sensing XII*, International Society for Optics and Photonics, Orlando, 4 June 2011